



## Preparation of $\text{La}_{0.7}\text{Ca}_{0.3}\text{Mn}_{0.95}\text{Fe}_{0.05}\text{O}_3$ perovskites by different methods: Catalytic activity towards the hydroxylation of benzene

Ahmed Imam Hanafy <sup>a,b,\*</sup>, Ibraheem Othman Ali <sup>b</sup>,  
Zeinhom Mohamed El-Bahy <sup>a,b</sup>, and Khaled Hussein Mahmoud <sup>c,d</sup>

<sup>a</sup> Chemistry Department, Faculty of Science, Taif University, 21985, Taif, Saudi Arabia

<sup>b</sup> Chemistry Department, Faculty of Science, Al-Azhar University, Nasr City, 11884, Cairo, Egypt

<sup>c</sup> Physics Department, Faculty of Science, Taif University, Taif, 21985, Saudi Arabia

<sup>d</sup> Physics Department, Faculty of Science, Cairo University, Cairo, 12612, Egypt

\*Corresponding author at: Chemistry Department, Faculty of Science, Taif University, 21985, Taif, Saudi Arabia.  
Tel.: +966.2.8322143; fax: +966.2.8322143. E-mail address: [ahmedih@yahoo.com](mailto:ahmedih@yahoo.com) (A.A. Hanafy).

### ARTICLE INFORMATION

Received: 16 March 2013  
Received in revised form: 07 June 2013  
Accepted: 08 June 2013  
Online: 30 September 2013

### KEYWORDS

XRD  
SEM  
Benzene  
Perovskites  
Hydroxylation  
Catalytic activity

### ABSTRACT

Nanoparticles of the  $\text{La}_{0.7}\text{Ca}_{0.3}\text{Mn}_{0.95}\text{Fe}_{0.05}\text{O}_3$  perovskites were synthesized by various wet chemical routes, namely, co-precipitation, oxalate-gel and citrate-gel methods. Phase formation and crystal structure of the synthesized powders were examined by the X-ray diffraction (XRD). The morphology was evaluated by the scan electron microscopy (SEM). Infrared transmission spectroscopy revealed that stretching and bending modes were influenced by the preparation methods. The citrate gel method yielded better powder properties. The prepared perovskite samples were used in the oxidation of benzene. The highest activity for the catalytic oxidation of benzene to phenol in presence of hydrogen peroxide ( $\text{H}_2\text{O}_2$ ) was obtained with the citrate-gel prepared sample.

### 1. Introduction

Much research effort has been devoted in recent years to composites containing manganese oxide to take advantage of their interesting properties, i.e. metal to insulator transition and colossal magneto resistance (CMR). Doped manganites, with general formula of  $\text{Ln}_{1-x}\text{Ca}_x\text{MnO}_3$  have been intensively studied, since they are considered as potential candidates for industrial applications [1]. Increased attention has been given to the compound  $\text{La}_{1-x}\text{Ca}_x\text{MnO}_3$ , where the ions  $\text{La}^{3+}$  and  $\text{Ca}^{2+}$  have very similar ionic radius, e.g. 1.36 and 1.38 Å, respectively [2]. The calcium doped  $\text{LaMnO}_3$  manganites have mixed valence of  $\text{Mn}^{3+}/\text{Mn}^{4+}$  with the configuration  $(t_{2g})^3(e_g)_1$  for  $\text{Mn}^{3+}$  and  $(t_{2g})^3$  for  $\text{Mn}^{4+}$ . By changing the ratio La/Ca and by varying the temperature, the transport properties of the  $\text{La}_{1-x}\text{Ca}_x\text{MnO}_3$  materials can be tuned from insulating to metallic state [3]. The magnetic properties can vary from paramagnetic, ferromagnetic to antiferromagnetic by changing the doped ions in the cationic site and its ratio. In the ferromagnetic region, corresponding to a doping range of  $0.3 < x < 0.7$ , a drop in the resistivity has been observed at the transition point from metal to semiconductor followed by the colossal magnetoresistive effect (CMR) [4]. Traditionally, these mixed oxides have been prepared through a calcination-milling (CM) procedure, which results in low surface area and poor active sites materials. To overcome this limit, several techniques were developed, one of which is citrate or tartrate sol-gel (SG) method. SG allows to generate relatively high surface area, up to two orders of magnitude higher than for the samples prepared by CM [5,6]. Indeed, the formation of the citrate or tartrate complex keeps the cations homogeneously dispersed, allowing obtaining the

pure perovskitic phase at low calcinations temperatures (ca. 500-600 °C). Thus the catalytic activity of the samples prepared by SG methods is usually higher than that of the samples prepared by other methods.

It is well known that the catalytic oxidation of hydrocarbons is supposed to occur on perovskite surface by means of the redox mechanism in which the oxygen on the catalyst are partly consumed by hydrocarbons and then regenerated by means of uptake from gaseous phase during a continuous cycle [7,8]. Fluctuation of the Mn cation between two stable oxidation states ( $\text{Mn}^{3+} \rightleftharpoons \text{Mn}^{4+}$ ) is of a considerable importance for the progress of this mechanism. At high temperature, the oxidation process involves lattice oxygen as active species for substituted as well as unsubstituted samples. This mechanism is connected to the presence of lattice species in the layers near to the surface. Then, the evolution of these species was attributed to the reduction of the Mn site cations to lower oxidation state [9,10]. Nevertheless, the intrinsic activity of the perovskite is difficult to be clearly evidenced because of the relatively low specific surface areas and/or the presence of undesired impurities like carbonates or oxides (e.g.  $\text{Co}_3\text{O}_4$ ) [11-13]. These two parameters strongly depend on the preparation method as well as the calcination procedure for achieving the crystallized perovskite phase. Citrate method is probably the most widespread and the most effective route to create catalysts of higher surface area. Additionally, the decomposition of the amorphous citrate precursors leads to mixed oxides or solid solutions of high homogeneity [14] contrary to methods using hydroxide precursors for instance [15].

The aim of this work was to prepare  $\text{La}_{0.7}\text{Ca}_{0.3}\text{Mn}_{0.95}\text{Fe}_{0.05}\text{O}_3$  perovskites using the different preparation methods (citrate, oxalate and co-precipitated methods). The samples were characterized by XRD, FT-IR spectroscopy and SEM techniques. Also, the catalytic activity of the prepared samples will be evaluated towards the hydroxylation of benzene and establish relationships with their physicochemical properties.

## 2. Experimental

### 2.1. Materials

Lanthanum chloride, manganese nitrate, calcium nitrate, iron nitrate, citric acid, oxalic acid, ammonium carbonate, ethylenglycol were purchased from Merck company. Benzene, hydrogen peroxide, ammonium hydroxide, 4-amino-antipyrine, potassium ferrocyanate were purchased from Sigma Company. All the chemicals used in this work were analytical grade.

### 2.2. Preparation of perovskites by sol gel methods

#### 2.2.1. Gel-citrate complexation route (GC sample)

The perovskites particles were prepared by the citrate precursor method. Briefly, the gel precursor was prepared by dissolving 0.7 mol  $\text{LaCl}_3 \cdot 5\text{H}_2\text{O}$ , 0.3 mol  $\text{Ca}(\text{NO}_3)_2$ , 0.95 mol  $\text{Mn}(\text{NO}_3)_2$ , 0.05 mol  $\text{Fe}(\text{NO}_3)_3 \cdot 9\text{H}_2\text{O}$  and 0.2 mol  $\text{C}_6\text{H}_8\text{O}_7 \cdot \text{H}_2\text{O}$  as quilting agent in 400 mL of deionized water. The solution was stirred for 1 h at 80 °C. Ethylenglycol (0.1 mol) was added to the previous solution with continuous stirring until a viscous gel was formed and the resulting gel was evaporated till dryness. The obtained powder was ground, and finally annealed at 900 °C for 12 h.

#### 2.2.2. Gel-oxalate complexation route (GO sample)

Stoichiometric amounts of  $\text{LaCl}_3 \cdot 5\text{H}_2\text{O}$ ,  $\text{Ca}(\text{NO}_3)_2$ ,  $\text{Mn}(\text{NO}_3)_2$  and  $\text{Fe}(\text{NO}_3)_3 \cdot 9\text{H}_2\text{O}$  were dissolved in distilled water. Then a solution of oxalic acid in water was added to the metal solution with vigorous stirring. The oxalic acid/metal ions ratio (La, Ca, Mn, and Fe) was fixed at 2:0.7:0.3:0.95:0.05, respectively. The solution was stirred at 80 °C for 1 h and then ethylene glycol (0.1 mol) was added to the previous solution with continuous stirring until a viscous gel was formed. The resulting gel was evaporated till dryness and the obtained powder was ground to form fine powders. The powders were pressed and then annealed at 900 °C for 12 h.

#### 2.2.3. Co-precipitation route (CP samples)

Stoichiometric amounts of  $\text{LaCl}_3 \cdot 5\text{H}_2\text{O}$ ,  $\text{Ca}(\text{NO}_3)_2$ ,  $\text{Mn}(\text{NO}_3)_2$  and  $\text{Fe}(\text{NO}_3)_3 \cdot 9\text{H}_2\text{O}$  were dissolved in water under vigorous stirring for 1 h at 70 °C. A solution of ammonium carbonate was added dropwise to the previous solution forming carbonate precipitates. The precipitates were filtered and the mother liquor was checked for complete precipitation by adding few drops of ammonium carbonate. Afterwards, the precipitate was filtered, dried at 120 °C for 4 h. The powder was finally calcined at 900 °C for 12 h.

### 2.3. Physico-chemical characterizations

Powder XRD data of the prepared samples were measured at room temperature using Philips diffractometer (type PW 3710). The patterns were run with Ni-filtered copper radiation ( $\lambda = 1.5404 \text{ \AA}$ ) at 30 kV and 10 mA with a scanning speed of  $2\theta = 2.5^\circ/\text{min}$ . The size of the crystallographic grain has been deduced by applying the Scherrer formula  $D = 0.89\lambda/\beta \cdot \cos\theta$  [16], where  $D$  is the crystallite size,  $\lambda$  represents the X-ray wavelength (1.5404 Å),  $\beta$  is the full width at half the maximum intensity (FWHM) in radians, and  $\theta$  is the Bragg's angle.

Scanning electron micrographs (SEM) were obtained on a Joel scanning microscope model JSM5410 operated at 15 kV. The sample was deposited on a sample holder with an adhesive carbon foil and sputtered with gold.

### 2.4. Catalytic tests

The hydroxylation of benzene in presence of  $\text{H}_2\text{O}_2$  was used to evaluate the catalytic activity of the prepared samples. The reaction was carried out in a solvent-free three-phase slurry reactor system. This liquid phase reaction was conducted in a 250 mL batch glass reactor equipped with a condenser under atmospheric pressure. A hotplate-magnetic stirrer with variable speed and an oil bath were used for stirring and heating the mixture. The catalyst was dried at 110 °C before using. A typical reaction mixture contained 0.1 g of catalyst, 50 cm<sup>3</sup> of benzene (99.7%) and 2 mL of  $\text{H}_2\text{O}_2$  (30% wt/wt) was added drop wise during 30 min with stirring to about 70 min. Then, the concentration of phenol was determined at  $\lambda_{\text{max}} = 510 \text{ nm}$  using UV-Vis spectrophotometer by the 4-aminoantipyrine method [17,18]. After reaction, a sample of 5 mL of reaction mixture was withdrawn and filtered. 0.5 mL of 4-aminoantipyrine was added into supernatant solution which was followed by adding 0.5 mL of  $\text{K}_3[\text{Fe}(\text{CN})_6]$  to the same mixture. After 15 min, the absorption at  $\lambda_{\text{max}} = 510 \text{ nm}$  was determined and the concentration of phenol was measured.

## 3. Result and discussion

### 3.1. Phase homogeneity

Figure 1 shows the XRD patterns of the prepared samples by the three investigated synthetic methodologies. All the samples provide the presence of the perovskite rhombohedral structure  $\text{La}_{0.7}\text{Ca}_{0.3}\text{Mn}_{0.95}\text{Fe}_{0.05}\text{O}_3$  [19]. For clarity, the expansion at  $2\theta = 31\text{-}35^\circ$  range is shown in Figure 2. The peaks appeared at  $2\theta = 18.37$  and  $22.95^\circ$  are related to the perovskite phase as superstructure reflections such as (101 and 110) [20]. The material prepared via gel-oxalate (GO samples), Figure 1a, shows single-phase character with the presence of weak diffraction peak at  $2\theta = 36.06, 44.4$  and  $62.1^\circ$  due to the precipitation of very small amount of cubic  $\text{Mn}_3\text{O}_4$  [JC-PDF #75-1560]. This indicates that the GO process under the adopted conditions is not able to produce a homogeneous material and the rhombohedral phase of  $\text{La}_{0.7}\text{Ca}_{0.3}\text{Mn}_{0.95}\text{Fe}_{0.05}\text{O}_3$  is formed by solid state reaction of the constituents of the combustion "ashes". Notably, the gel-oxalate process has been widely used to prepare  $\text{LaNi}_x\text{Fe}_{1-x}\text{O}_3$  nanoparticles with good phase homogeneity [21]. Therefore, for  $\text{La}_{0.7}\text{Ca}_{0.3}\text{Mn}_{0.95}\text{Fe}_{0.05}\text{O}_3$  sample, we can not exclude that the synthetic conditions, such as oxalic/metal ions ratio, can be further optimized leading to homogenous materials. Phase homogeneity of the prepared samples was studied by comparison with structural data reported in the literature [22,23].  $\text{La}_{0.7}\text{Ca}_{0.3}\text{Mn}_{0.95}\text{Fe}_{0.05}\text{O}_3$ , like all the  $\text{La}_{1-x}\text{Ca}_x\text{MnO}_3$  systems with  $x < 0.5$ , crystallizes in a rhombohedral structure (R3c space group). The rhombohedral distortion of the ideal perovskite octahedra is characterized by the splitting of the principal reflection, which appears as a double peak in the range  $2\theta = 32\text{-}34^\circ$ .

The materials prepared through GC and CP samples routes present the desired phase even after calcination at low temperature: the fit of the XRD patterns of the GC and CP samples is in a good agreement with the rhombohedral structure of  $\text{La}_{0.7}\text{Ca}_{0.3}\text{Mn}_{0.95}\text{Fe}_{0.05}\text{O}_3$ . This result is consistent with the statistical distribution of the cations in the resin produced by the GC synthesis and in the mixed hydroxides produced by the CP synthesis, which is maintained in the final materials. A careful analysis of the two important diffraction peaks ( $2\theta = 33$  and  $57^\circ$ ) shows the changes in the crystalline structure of this series. A close up of the signal corresponding to  $2\theta = 33^\circ$  is also shown in Figure 2. It can be observed that the

two signals studied for the perovskites prepared with GO are singlets. The first, at  $33^\circ$  is acute and intense, while the one at  $57^\circ$  is wide and of much less intensity, typical of orthorhombic structures [19]. The crystallite size of the prepared solids were calculated using Scherrer's equation [16] and it was calculated by average crystal size for the intense line at  $2\theta(22.87$  and  $46.75^\circ)$ ,  $(22.87, 32.41, 32.77$  and  $46.75^\circ)$  and  $(32.41, 32.77$  and  $46.75^\circ)$ . The average crystallite size was found to be 76.5, 97.2 and 98.3 nm for the samples prepared using oxalic acid, citric acid and Co precipitation method respectively. The lattice parameters, and unit cell volume were calculated and the data are listed in Table 1. The data show that the samples prepared by co-precipitation or citrate methods have the same lattice parameters.

**Table 1.** Structure parameters for  $\text{La}_{0.7}\text{Ca}_{0.3}\text{Mn}_{0.95}\text{Fe}_{0.05}\text{O}_3$  samples.

Samples	Cell parameters (Å)			V (Å <sup>3</sup> )
	a	b	c	
Co-precipitation	5.5160	5.5160	13.3557	351.9168
Citrate methods	5.5100	5.5100	13.3497	350.9939
Oxalate methods	5.4990	5.4990	13.3387	349.3058

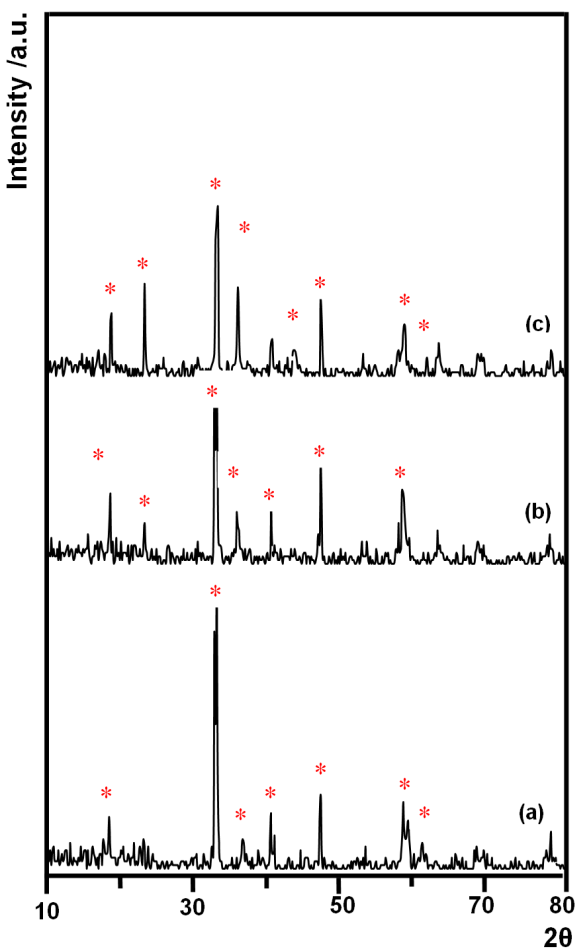


**Figure 1.** X-ray diffractograms of perovskite material prepared by different methods and calcined at  $900^\circ\text{C}$ . (a) Co-precipitation method, (b) Citrate method and (c) Oxalate method.

### 3.2. Scanning electron microscopy (SEM)

In order to observe the microstructure of the synthesized perovskites prepared by different methods, SEM analyses were performed and the images are shown in Figure 3a-c. The SEM micrographs exhibited foamy agglomerated particles with a

wide distribution and presence of large voids in their structure. The morphology of the samples showed that the particles are aggregated and pieces of gel were obtained, when using co-precipitation method and oxalate precursors, Figure 3a and 3b, respectively. The powders obtained starting with citrate showed more dispersion, Figure 3c. This result strongly supports that citrate methods plays a structure directing role enhancing the nucleation. The enhanced nucleation has thus led to the formation of smaller particle size.

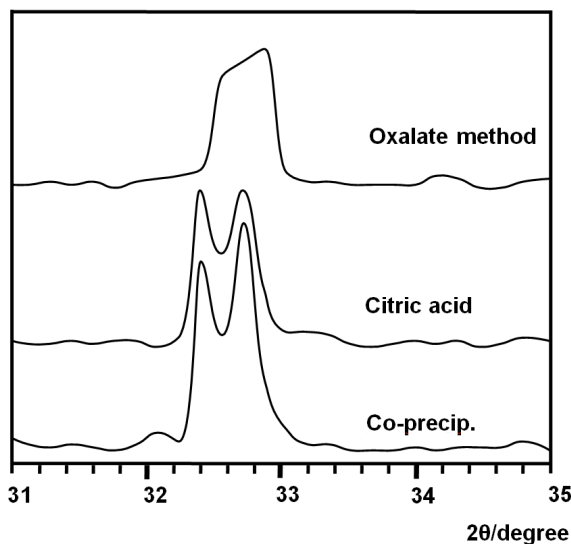


**Figure 2.** XRD spectra of  $\text{La}_{0.7}\text{Ca}_{0.3}\text{Mn}_{0.95}\text{Fe}_{0.05}\text{O}_3$  samples, collected after the calcination treatment at  $900^\circ\text{C}$ . As a reference, the position of the reflection of the cubic (JCPDF, card No. 750541) and orthorhombic (JCPDF, card No. 742203)  $\text{LaFeO}_3$  and cubic (JCPDF, card No. 330710) and rhombohedral (JCPDF, card No. 330711).

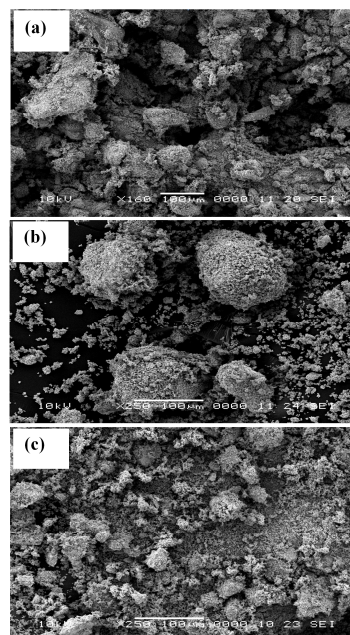


**Figure 3.** SEM images of different perovskite samples prepared by (a) Co-precipitation method; (b) Oxalate method and (c) Citrate method.

### 3.3. FT-IR spectroscopy

Figure 4 presents the IR spectra for all the perovskites in the range between  $4000$  and  $500\text{ cm}^{-1}$ . The wide band in the

range of 3400-3800  $\text{cm}^{-1}$  is due to the lengthening of the O-H bond in water due to the exposure to air and environmental humidity for the studied perovskites. The sample prepared by GC method showed small bands at 2988 and 2420  $\text{cm}^{-1}$ . According to Pecchi *et al.* [19], the former band is due to carbonated segregated  $\text{La}_2\text{O}_3$  phase while the other one is believed to be due to physisorbed  $\text{CO}_2$  on cationic species [24]. The most important band of the perovskites structure ( $\nu_1$ ) is observed at 630  $\text{cm}^{-1}$  which is the characteristic band of oxides with perovskite-type structure. The absorption peaks around  $\nu_3$  at  $\sim 630\text{cm}^{-1}$  and  $\nu_4$  at  $\sim 500\text{cm}^{-1}$  should belong to stretching ( $\nu_3$ ) and bending ( $\nu_4$ ) of the internal phonon modes of  $\text{MnO}_6$  octahedral [25-27]. The stretching mode is related to the change of Mn-O-Mn bond length and the bending mode involves the change of Mn-O-Mn bond angle. The appearance of the stretching and bending modes at transmission spectra indicates that the perovskite structure of LCMO has been formed at the temperature of 800 °C, which is in agreement with the results of XRD patterns as shown in Figure 1.

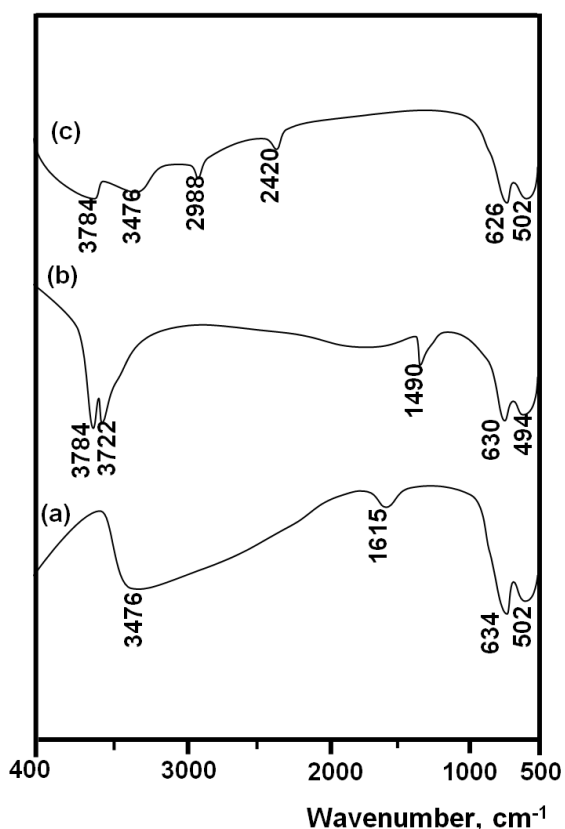


**Figure 4.** FT-IR spectra of perovskite prepared by (a) Co-precipitation method; (b) Oxalate method and (c) Citrate method.

### 3.4. Catalytic activity

Oxidation reaction on oxides are often described by means of the Mars and van Krevelen model [28,29] involving two step redox reaction mechanism. The first step is the reaction between the oxidisable reactant (hydrocarbon) and the active oxygen on the surface. The second step is the re-oxidation of the reduced surface site by gas phase oxygen. Indeed, the reaction sites are manganese ions ( $\text{Mn}^{3+}$  and  $\text{Mn}^{4+}$ ). So, at temperature slower than 100 °C, as the diffusion of oxygen ions ( $\text{O}^-$ ) into the lattice is inhibited, the redox reaction takes place at these sites by consuming and regenerating weakly adsorbed oxygen. Oxygen can be available to the combustion in combination with a temporary shift of Mn valence from 4+ back

to 3+. Manganese is re-oxidised by oxygen molecules coming from gaseous atmosphere. The rate determining step is supposed to be the rate of lattice oxygen diffusion which determines the amount of available active oxygen for the oxidation reaction. Figure 5 shows the progress of the conversion of benzene to phenol with time in presence of  $\text{H}_2\text{O}_2$ . The yield of phenol reaches the maximum value of 15.5, 20.7 and 35.4% over the three samples (Cp, OG and CG), respectively, at a reaction time of 60 min. The maximum conversion on the sample prepared by CG method may be related to the high homogeneity of this sample.

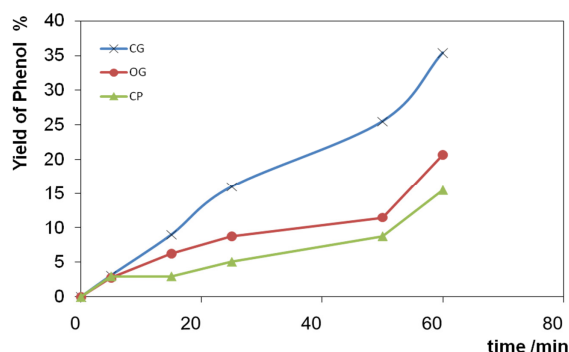


**Figure 5.** Yield of phenol produced using the solid samples prepared by different methods. Reaction conditions: atmospheric pressure, temperature 80 °C, catalyst 0.1 g, ratio of  $\text{H}_2\text{O}_2$  to benzene equal 0.0388 mole and 20 mL additional water.

The effect of  $\text{H}_2\text{O}_2$  amount on the yield of phenol over the citrate sample is shown in Figure 6.  $\text{H}_2\text{O}_2$  acts as the oxidant in the conversion of benzene to phenol. Thus, it is natural that no phenol is obtained in the absence of  $\text{H}_2\text{O}_2$  [30]. The variation of phenol yield with the amount of  $\text{H}_2\text{O}_2$  used gives the same tendency over the three catalysts used. The yield of phenol increases along with the increase of the amount of  $\text{H}_2\text{O}_2$  and reaches a maximum at 38.8 mmol (1.85 mol/L)  $\text{H}_2\text{O}_2$ . This corresponds to the molar ratio of  $[\text{H}_2\text{O}_2]/[\text{Benzene}]$  of about 1.7. A slight decrease in the yield of phenol was observed with further increase of the amount of  $\text{H}_2\text{O}_2$ . This may result from the further oxidation of the phenol formed. The stoichiometric ratio of  $\text{H}_2\text{O}_2$  to benzene for the hydroxylation reaction is 1:1, while the results show that the  $\text{H}_2\text{O}_2$  needed for the favorable phenol yield is about 1.7 times its stoichiometry. In fact, in the present reaction system, the benzene oxidation catalyzed is accompanied by the self-decomposition of hydrogen peroxide. Therefore, the excess of  $\text{H}_2\text{O}_2$  may be consumed in the deep oxidation or in its self-decomposition.

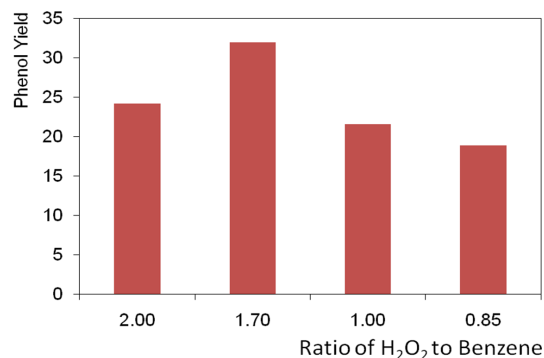


**Figure 6.** Hydroxylation of benzene as a function of molar ratio of benzene/ $\text{H}_2\text{O}_2$  using the sample prepared by citrate-gel method after 60 min of reaction progress. Reaction conditions: atmospheric pressure, temperature 80 °C, catalyst 0.1 g, 0.0388 mole of  $\text{H}_2\text{O}_2$  and x mole of benzene ( $x = 0.0194, 0.0228, 0.038$  and  $0.045$  mole) and 20 mL additional water.

#### 4. Conclusions

The nanoparticles  $\text{La}_{0.7}\text{Ca}_{0.3}\text{Mn}_{0.95}\text{Fe}_{0.05}\text{O}_3$  perovskites were prepared by the sol-gel process. The prepared samples were characterized by means of different tools and then used in the oxidation of benzene in the presence of  $\text{H}_2\text{O}_2$ . The sol-gel method using citric acid as chelating agent was found to be more useful way for the preparation of  $\text{La}_{0.7}\text{Ca}_{0.3}\text{Mn}_{0.95}\text{Fe}_{0.05}\text{O}_3$  perovskites than the other methods. The perovskite prepared by this method also was found to be the highest active catalyst in the oxidation of benzene. This indicates that catalytic activity correlates not only with the bulk structure of the perovskite phase and consequently oxygen mobility but also with the content of manganese and its surface concentration.

#### Acknowledgments

The authors acknowledge Taif University for supporting this work by Taif University research program (1-433-1694).

#### References

- [1]. Ahn, K. H.; Wu, X. W.; Liu, K.; Chien, C. L. *Phys. Rev. B* **1996**, *54*, 15299-15302.
- [2]. Canulescu, S.; Lippert, T. H.; Wokaun, A.; Robert, R.; Logvinovich, D.; Weidenkaff, A.; Dobeli, M.; Schneider, M. *Prog. Sol. Stat. Chem.* **2007**, *35*, 241-248.
- [3]. Ziese, M.; Semmelhack, H. C.; Han, K. H.; Sena, S. P.; Blythe, H. J. *J. Appl. Phys.* **2002**, *91*, 9930-9937.
- [4]. Zener, C. *Phys. Rev.* **1951**, *82*, 403-405.
- [5]. Zhang, H. M.; Teraoka, Y.; Yamazoe, N. *Chem. Lett.* **1987**, *16*, 665-668.
- [6]. Arai, H.; Yamada, T.; Eguchi, K.; Seiyama, T. *Appl. Catal.* **1986**, *26*, 265-276.
- [7]. Seiyama, T.; Tejuka, L. G.; Fierro, J. I. G. (Eds.), *Properties and Applications of Perovskite-type Oxides*, Marcel-Dekker, NY, 1993, pp. 215.
- [8]. Tejuka, L. G.; Fierro, J. L.; Tascon, J. M. D. *Adv. Catal.* **1989**, *36*, 237-248.
- [9]. Voorhoeve, R. J. H.; *Advanced Materials in Catalysis*, Academic Press, NY, 1977, pp. 129.
- [10]. Seiyama, T.; Yamazoe, N.; Eguchi, E. *Ind. Eng. Chem. Prod. Res. Dev.* **1985**, *24*, 19-27.
- [11]. Liang, J. J.; Weng, H. S. *Ind. Eng. Chem. Res.* **1993**, *32*, 2563-2572.
- [12]. Busca, G.; Daturi, M.; Finocchio, E.; Lorenzelli, V.; Ramis, G.; Willey, R. J. *Catal. Today* **1997**, *33*, 239-249.
- [13]. Royer, S.; Berube, F.; Kaliaguine, S. *Appl. Catal. A: Gen.* **2005**, *282*, 273-284.
- [14]. Alifanti, M.; Kirchnerova, J.; Delmon, B. *Appl. Catal. A: Gen.* **2003**, *245*, 232-243.
- [15]. Barnard, K. R.; Foger, K.; Turney, T. W.; Williams, R. D. *J. Catal.* **1990**, *125*, 265-275.
- [16]. Bragg, W. H.; Bragg, W. L. *Nature* **1913**, *91*, 557-560.
- [17]. Greenberg, A. E.; Clesceri, L. S.; Eaton, A. D. (Eds.), *Standard Methods for the Examination of Water and Wastewater*, 17<sup>th</sup>ed., American Public Health Association (APHA), Washington, DC, 1989.
- [18]. Tor, A.; Cengeloglu, Y.; Aydin, M. E.; Ersoz, M. *J. Colloid Interface Sci.* **2006**, *300*, 498-503.
- [19]. Pecchi, G.; Campos, C.; Pena, O.; Cadus, L. E. *J. Mol. Catal. A* **2008**, *282*, 158-166.
- [20]. Bashir, J.; Shaheen, R.; Siddique, M.; Azad, A. K.; Eriksen, J.; Rundlof, H. *J. Physica B* **2006**, *385-386*, 126-129.
- [21]. Bontempi, E.; Garzella, C.; Valetti, S.; Depero, L. E. *J. Eur. Ceram. Soc.* **2003**, *23*, 2135-2142.
- [22]. Rousseau, S.; Loridant, S.; Delichere, P.; Boreave, A.; Deloume, J. P.; Vernoux, P. *Appl. Catal. B* **2009**, *88*, 438-447.
- [23]. Kundaliya, D. C.; Vija, R.; Kulkarnia, R. G.; Tulapurkar, A. A.; Pinto, R.; Malik, S. K.; Yelon, W. B. *J. Magn. Mater.* **2003**, *264*, 62-69.
- [24]. Liu, L.; Liu, B.; Dong, L.; Zhu, J.; Wan, H.; Sun, K.; Zhao, B.; Zhu, H.; Dong, L.; Chen, Y. *Appl. Catal. B* **2009**, *90*, 578-586.
- [25]. Yang, W. D.; Chang, Y. H.; Huang, S. H. *J. Eur. Ceram. Soc.* **2005**, *25*, 3611-3618.
- [26]. Nagabhushana, B. M.; Chakradhar, R. P. S.; Ramesh, K. P.; Prasad, V.; Shivakumara, C.; Chandrappa, G. T. *Physica B* **2008**, *403*, 3360-3364.
- [27]. Rostamnejadi, A.; Salamati, H.; Kameli, P.; Ahmadvand, H. *J. Magn. Mater.* **2009**, *321*, 3126-3131.
- [28]. Mars, P.; Krevelen, D. V. *Chem. Eng. Sci. Suppl.* **1954**, *3*, 41-59.
- [29]. Hammami, R.; Ben Aissa, S.; Batis, H. *Appl. Catal. A* **2009**, *353*, 145-153.
- [30]. Chammingkwan, P.; Hoelderich, W. F.; Mongkhonsi, T.; Kanchanawanichakul, P. *Appl. Catal. A* **2009**, *352*, 1-9.